Neuroradiology
https://doi.org/10.1007/s00234-021-02698-8

FUNCTIONAL NEURORADIOLOGY

# The topology of ventricle surfaces and its application in the analysis of hydrocephalic ventricles: a proof-of-concept study

Yu Tung Lo[1] · Sumeet Kumar[2] · Leanne Qiaojing Tan[1] · Christine Lock[1] · Nicole Chwee Har Keong[1,3]

Received: 29 November 2020 / Accepted: 22 March 2021


## Abstract

**Purpose** The cerebral ventricles deform in a non-uniform fashion in response to increased CSF volume and/or pressure in hydrocephalic syndromes. Current research is focused on volumetric analyses, while topological analysis of ventricular surfaces remains understudied. We developed a method of quantitatively modeling the curvature of ventricular surfaces to analyze changes in ventricular surfaces in normal pressure hydrocephalus (NPH) and Alzheimer's disease (AD), using the left frontal horn as an example.

**Methods** Twenty-one patients with NPH were recruited from our institution, and 21 healthy controls (HC) and patients with Alzheimer's disease (AD) were identified from the Alzheimer's Disease Neuroimaging Initiative (ADNI) database. On T1-weighted fine-cut magnetic resonance sequences, 3D Slicer was used to segment the left frontal horn. Next, the mean curvatures at a set of points on the ventricular surface were determined. The frontal horns were scaled and centered into normalized volumes, allowing for pooling across the study subjects. The frontal horn was divided into superolateral, superomedial, inferolateral, and inferomedial surfaces, and locoregional mean curvatures were analyzed. Statistical comparisons were made between NPH, AD, and HC groups.

**Results** Significant differences in the mean curvature of lateral surfaces of the ventricles distinguished patterns of distortion between all three cohorts. Significant flattening of the superomedial surface discriminated NPH from HC and AD. However, significant rounding of the inferomedial surface compared to controls was a distinguishing feature of NPH alone.

**Conclusion** NPH ventricles deform non-uniformly. The pattern of surface distortion may be used as an additional tool to differentiate between these hydrocephalic conditions.

**Keywords** Normal pressure hydrocephalus · NPH · Hydrocephalus · Morphology · Topology · Curvature · ADNI

## Introduction

The cerebral ventricle can be regarded as a deformable fluid vessel. Periventricular structures of varying degrees of compliance constrain the ability of the ventricle to deform in response to an increase in cerebrospinal fluid (CSF) volume and/or pressure. Information about parenchymal compliance and pressure on adjacent structures can be inferred from the pattern of locoregional deformation of specific ventricular segments. Conventionally, the degree of hydrocephalus is quantified using two-dimensional indices such as the Evans' index and callosal angle, which have utility in the diagnosis of normal pressure hydrocephalus (NPH), with some capacity for prediction of shunt responsiveness [1, 2, 3, 4]. Two-dimensional indices, with or without volumetric analyses, have been the focus of previous studies of ventricular enlargement in hydrocephalus; quantitative changes in ventricular morphology have remained understudied [4, 5, 6, 7].

While the ventricles are initially able to accommodate an increase in CSF volume with little increase in pressure, the ventricular system eventually exhausts its capacity for distension, resulting in surface distortion. This deformation has been observed to occur in a non-uniform manner, with certain segments of the ventricular system more deformable than others. The non-uniform deformation of the ventricles may therefore cause variable distortion in the overlying subcortical

✉ Nicole Chwee Har Keong
nchkeong@cantab.net

[1] Department of Neurosurgery, National Neuroscience Institute, 11 Jalan Tan Tock Seng, Singapore 308433, Singapore

[2] Department of Neuroradiology, National Neuroscience Institute, 11 Jalan Tan Tock Seng, Singapore 308433, Singapore

[3] Duke-NUS Medical School, 8 College Road, Singapore 169857, Singapore

Published online: 15 April 2021

structures. In our previous work, we have demonstrated that an "at-risk" model of white matter injury, comprising six key regions-of-interest, can demonstrate at least three concurrent and distinct patterns of injury in NPH [8]. The differing patterns of injury likely reflect the neuroanatomical arrangement of white matter fibers, and their proximity to the ventricles, i.e., to the risk of distortion due to progressive ventriculomegaly.

In the cerebral mantle, the appearance of mechanical stresses has also been thought to account for the phenomenon of diaschisis, i.e., that sudden neurophysiological or function changes in the brain can occur in areas remote to the brain lesions inciting such changes. In a study of a patient who developed a transient hemispatial neglect syndrome following surgical drainage of a large right frontotemporal arachnoid cyst, Pena et al. used a combination of finite element analysis and positron-emission tomography imaging to demonstrate that substantial shear and compressive stress concentrations with hypoperfusion were found in the parietal lobe, suggestive of brain deformation with the appropriate clinical sequelae [9]. Such dramatic findings of clinical changes with surgical intervention are rare but reported throughout the management of arachnoid cysts and disorders of CSF circulation. Nevertheless, in NPH and other chronic hydrocephalic syndromes, to our knowledge, the surface topology of the ventricular system has not been characterized.

In this study, we aimed to describe a method of quantifying the surface curvature of the ventricles using a semi-automatic segmentation technique. We applied this technique to evaluate the difference in ventricular morphology, using the left frontal horn as an example, between patients with NPH compared to those with Alzheimer's disease (AD) and healthy controls.

## Methods

### Data source

Twenty-one patients who met published criteria for probable or possible NPH [10], and were undergoing extended CSF drainage, were recruited prospectively from our institution. They had pre-intervention magnetic resonance imaging (MRI) scans. All NPH patients had ventriculomegaly with Evans' index ≥0.30 or bicaudate index ≥0.25, and had one or more features of the NPH triad of gait disturbance, cognitive impairment, and urinary incontinence. Some of them had overlay from other neurodegenerative conditions but did not meet diagnostic criteria for Alzheimer's and Parkinson's diseases, and/or had limited response to treatment. The study was approved by the National Healthcare Group Domain Specific Review Board (Ref 2014/00838) and the SingHealth Centralised Institutional Review Board (Ref 2016/2627). Informed consent was obtained from all participants, or their legal representatives when applicable. T1-weighted baseline scans for 21 healthy controls (HC) and 21 patients with AD were retrieved from the Alzheimer's Disease Neuroimaging Initiative (ADNI) database (adni.loni.usc.edu). These HC and AD subjects were randomly selected for comparison with the NPH group, with similar ages across the cohorts (NPH: mean 71, SD 6; AD: mean 73, SD 9; HC: 73, SD 3). AD patients had mild AD, meeting NINCDS-ADRDA criteria for probable AD and a Clinical Dementia Rating of 0.5 or 1.0 [11, 12, 13]. The ADNI was launched in 2003 as a public-private partnership, led by Principal Investigator Michael W. Weiner, MD. The primary goal of ADNI has been to test whether serial magnetic resonance imaging (MRI), positron-emission tomography (PET), other biological markers, and clinical and neuropsychological assessment can be combined to measure the progression of mild cognitive impairment (MCI) and early Alzheimer's disease (AD).

NPH participants were scanned in a 3T scanner (Ingenia, Philips Medical Systems, Best, Netherlands). Three-dimensional axial T1-weighted imaging with sensitivity encoding (SENSE) was acquired (TR = 7.3 ms, TE = 3.3 ms, flip angle = 8°, FOV = 256 × 256 mm, voxel size = 1.0 × 1.0 × 1.0 mm). Participants unable to undergo scans at 3T due to safety concerns were scanned at 1.5T at equivalent specifications. ADNI, AD, and HC participants were scanned in a 3T MRI scanner (GE Healthcare, Philips Medical Systems, or Siemens Healthcare, depending on the ADNI scanning site). MRI scanning protocols for each scanner model are available online (http://adni.loni.usc.edu/methods/documents/mri-protocols/).

### Ventricular segmentation

Ventricular segmentation was performed using a semi-automatic method in the open-source 3D Slicer software [14]. In brief, segmentation was performed on 1-mm fine-cut T1-weighted sequences. The ventricles were segmented using a combination of threshold-based identification of voxels with CSF-intensity signal, followed by manual editing and refinement of segments. For each patient, the left frontal horn was isolated. In this study, the frontal horn was defined as the region of the lateral ventricle anterior to the foramen of Monro.

### Surface modeling

We followed a previously described method of representing biological surfaces derived from imaging as a triangular meshwork of points [15, 16]. Briefly, the geometric relationships between the points are modeled with a mesh of tessellating triangles each formed from three adjacent points (or vertices). Next, a custom program created in the *Python* language (Python Software Foundation, Wilmington, DE) was used to

compute the mean curvature of the ventricular segments for each point on the surface. The program utilized the open-source module, *vtkplotter* [17]. The *.stl* files generated from the 3D Slicer were imported into the *Python* software for further processing and analysis.

Ventricles were normalized by scaling the left frontal horns to the volume of an average left frontal horn in a healthy control (HC). Next, the surface of the ventricle was downsampled to approximately 2000 points (with a small rounding error) using an algorithm based on a quadric error measure; briefly, the algorithm reduces the number of points representing a surface iteratively while seeking to minimize the deviation from the original surface ("quadric error measure") and thereby preserving the original curvature [18]. Downsampling standardized all ventricular surfaces to the same number of points (vertices) to enable comparisons, as well as smoothened the ventricular surfaces to minimize local irregularities and imaging artifacts.

## Curvature analysis

The method of curvature analysis was inspired by published works on cardiac ventricular analysis [15, 16, 19]. Curvature is defined as the reciprocal of the radius of the best fitting circle for a specified segment of an arc, with a dimension of length$^{-1}$.

Mean curvature, $H$, of a smooth surface is geometrically defined as [20, 21, 22]:

$$H = \frac{1}{2\pi}\int_0^{2\pi} \kappa(\theta)d\theta, \quad \kappa$$

: curvature along a specific angle $(\theta)$

A positive curvature denotes a convex surface, whereas a negative curvature denotes a concave surface. A flat surface has zero mean curvature. The larger the magnitude, the sharper the curvature. Using triangular mesh approximation (Fig. 1a and b) [23], the differential surface geometry can be simplified to discrete Euclidean geometry by taking the scaled average of all dihedral angles between two adjacent triangular faces around a vertex (illustrated in Fig. 1c). This is mathematically defined by [20, 24]:

$$H_{\text{vertex}} = \frac{1}{n}\sum_{i=1}^{n} H_{\text{edge}}(i),$$

$$\text{where } H_{\text{edge}}(i) = \frac{1}{6} \times \text{length of edge(i)} \times \text{dihedral angle(i)},$$

$$n = \text{number of edge neighbors}$$

The mean curvature, with a unit of cm$^{-1}$, was then normalized by scaling to the average volume of the frontal horn as determined from the HC cohort. This eliminated the effect of volume differences between individuals and enabled the pooling of measurements from different individuals.

Each frontal horn was divided into four quadrants—superolateral (SL), superomedial (SM), inferolateral (IL), and inferomedial (IM)—for regional analysis (Fig. 2). The quadrants were determined by two bisecting planes, one bisecting the superior and inferior compartments into two equal volume segments, and one bisecting the medial and lateral compartments into two equal volume segments. This methodology was chosen as a simple and easily reproducible way to subsection the frontal horn which could be automatically performed by the program. The posterior surface was truncated (the last 0.05 cm was excluded from analyses) as it represented an artificial boundary generated during segment generation between the frontal horn and the rest of the lateral ventricle.

## Pilot simulation tests with spheres and ellipsoids

In order to check the validity of the program, pilot tests were performed on simple geometric shapes, namely spheres and ellipsoids.

The first test was performed to visualize the behavior of how mean curvature changed with volume normalization (Fig. 3). Three spheres of different radii (1 cm, 2 cm, and 3 cm) and three ellipsoids belonging to different geometric classes (a prolate, an oblate, and a tri-axial ellipsoid) were used; for the latter, radii were varied between 1 cm, 2 cm, and 3 cm to achieve the above geometric configurations. Volume-normalized variants of the six shapes above were generated, by scaling to the volume of a sphere with a 1-cm radius. Volumes computed from the mesh (mesh volume) were compared to the actual geometric volume calculated mathematically. All figures were standardized to be represented by 1000 point coordinates. The mean curvature distributions along these surfaces were then represented by box-and-whisker plots (Fig. 4).

The second test was to verify the stability of mean curvature distribution to the reduction in the number of point coordinates representing the surface (i.e., the mesh density). Violin plots were used to visualize the mean curvature distributions (Fig. 5). Wireframe diagrams and reconstructed surface diagrams were presented to visualize the effect of reducing mesh density on surface curvature measurement.

## Curvature ratio (*R*)

The relative degree of curvedness between the ventricle in disease conditions (NPH, AD) can be expressed as a ratio relative to the mean curvature in the HC cohort. We termed this the curvature ratio, $R$. Therefore, $R_{\text{NPH}}$ is defined as median $H$ in the NPH cohort divided by the median $H$ in the HC

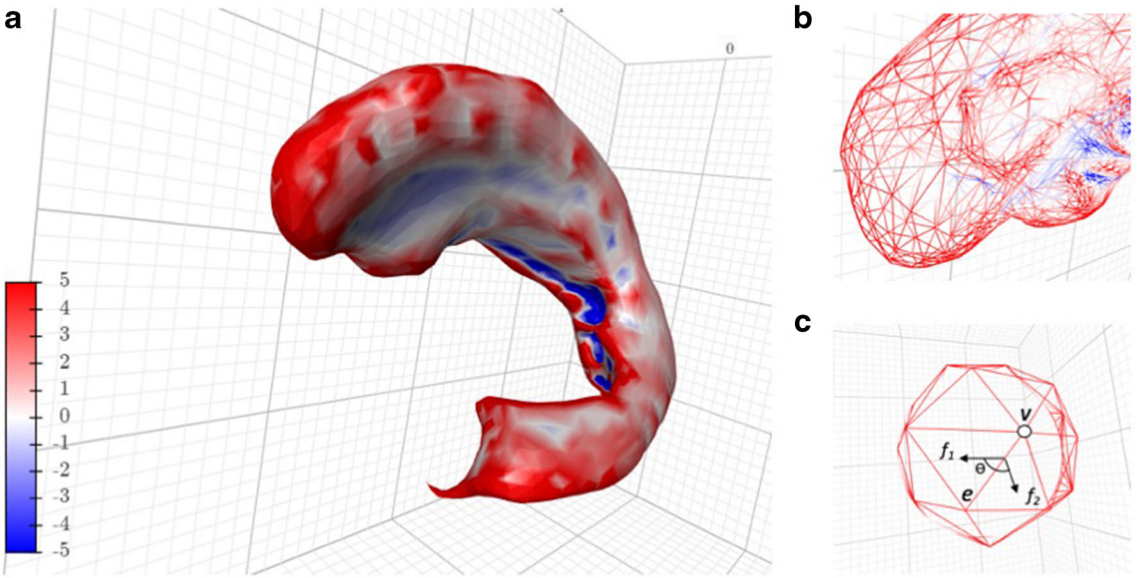


**Fig. 1** Representation of left ventricle. **a** Three-dimensional graphical visualization of the left frontal horn in one of the NPH patients. The mean curvature (normalized) at each point is represented by a color spectrum from red (a convex curvature of 5 units) to blue (a concave curvature of −5 units). White denotes a flat mean curvature at the respective local regions (a curvature of 0 unit). **b** In order to simplify graphical rendering and computation of mean curvatures, the ventricular surfaces are represented by a series of points in a three-dimensional Cartesian space. In addition, spatial relations between these points are represented by a mesh of tessellating triangles, each created by adjoining three adjacent points. **c** An illustration of how mean curvatures were calculated, using a dome as an example. The dihedral angle ( ) is the angle between the normal vector of the two neighboring triangular faces ($f_1$ and $f_2$). A vertex ($v$) is surrounded by a variable number of triangular planes, and the arithmetic mean of all edge ($e$) curvatures around the vertex estimates the mean curvature at the vertex

cohort. Similarly, $R_{AD}$ is defined as median $H$ in the AD cohort divided by the median $H$ in the HC cohort.

## Statistical analysis

The *Python* language was used to implement the image analysis and statistical analysis modules. The mean curvatures were pooled across all patients within their respective groups (that is, HC, NPH, and AD), and represented by box-and-whisker plots. Curvature values of more than 10 $cm^{-1}$ (i.e., corresponding to the curvature of small circles with radii <1 mm) were excluded as they were likely contour artifacts with no biological significance. The Mann-Whitney $U$ test with Bonferroni adjustment was used to compare curvature distributions between the groups. Statistical significance was defined as $p < 0.05$.

## Results

The left frontal horns of 21 HC, 21 NPH, and 21 AD patients were analyzed. For this pilot study, clinical characteristics were not evaluated.

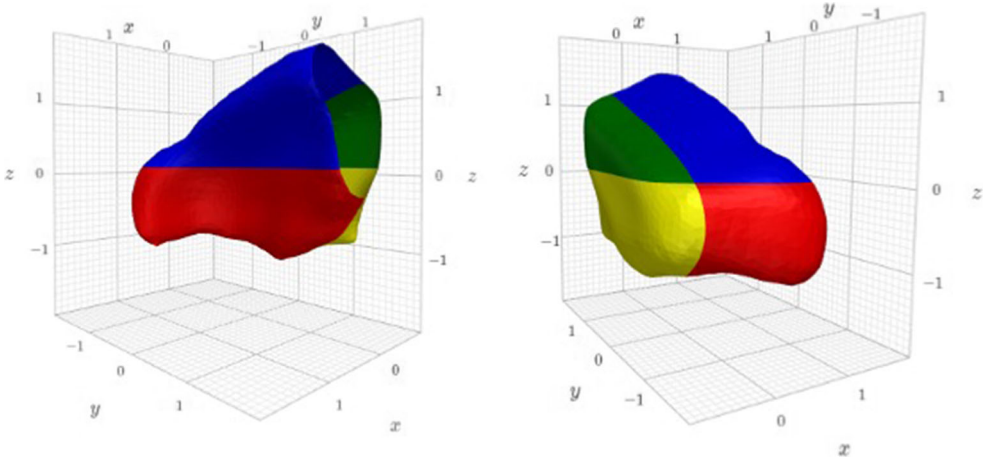

**Fig. 2** Ventricular surfaces are divided into four quadrants. The regional surfaces are named: superomedial (SM; green), superolateral (SL; blue), inferomedial (IM; red), and inferolateral (IL; yellow). The quadrants were constructed by the intersection of two planes, one dividing the superior and inferior segments into two regions with equal volumes, and one dividing the medial and lateral segments into two regions with equal volumes. Regional analysis was performed for each of the four quadrants

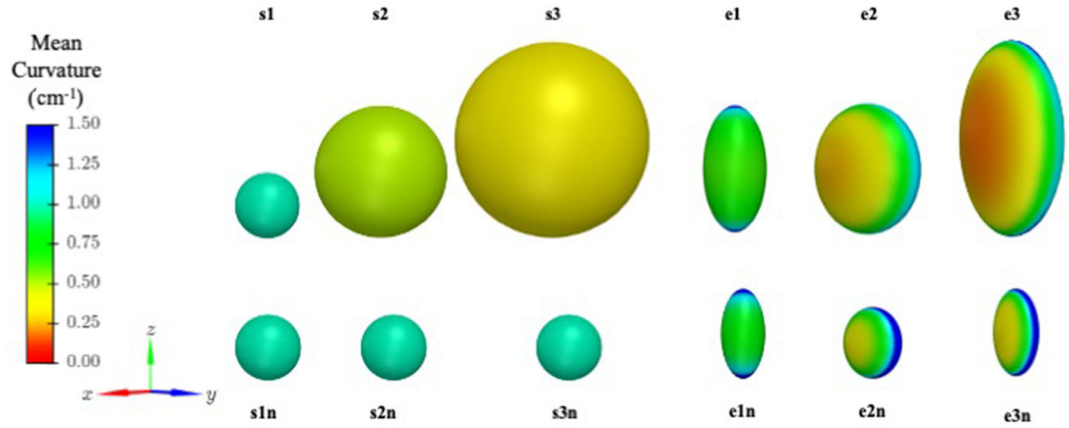


| | | Sphere 1 (s1) | Sphere 2 (s2) | Sphere 3 (s3) | Ellipsoid 1 (e1) | Ellipsoid 2 (e2) | Ellipsoid 3 (e3) |
|---|---|---|---|---|---|---|---|
| Actual | Radius (cm) | | | | | | |
| | x | 1 | 2 | 3 | 1 | 1 | 1 |
| | y | 1 | 2 | 3 | 1 | 2 | 2 |
| | z | 1 | 2 | 3 | 2 | 2 | 3 |
| | Mesh volume ($cm^3$) | 4.16 | 33.26 | 112.25 | 8.31 | 16.63 | 24.94 |
| | Geometric volume ($cm^3$) | 4.19 | 33.51 | 113.10 | 8.38 | 16.76 | 25.13 |
| | Number of point coordinates | 1000 | 1000 | 1000 | 1000 | 1000 | 1000 |
| Normalized | | **s1n** | **s2n** | **s3n** | **e1n** | **e2n** | **e3n** |
| | Mesh volume ($cm^3$) | 4.16 | 4.16 | 4.16 | 4.16 | 4.16 | 4.16 |
| | Number of point coordinates | 1000 | 1000 | 1000 | 1000 | 1000 | 1000 |

**Fig. 3** Validation of the calculations of volume and curvature parameters using test spheres and ellipsoids. Volumes were measured as mesh volume (mesh not shown) and compared to geometric volume calculated mathematically. Spheres of different radius were used: 1 cm (sphere 1; s1), 2 cm (sphere 2; s2), and 3 cm (sphere 3; s3). For a sphere of radius of 1 cm, the mean curvature is (1/1 cm) = 1 $cm^{-1}$ and is by definition uniform throughout the entire surface. Ellipsoids can be described by specifying the radius in each of the three cardinal planes ($x$, $y$, $z$). Ellipsoid 1 (prolate; e1) has two short axes and one long axis, ellipsoid 2 (oblate; e2) has one short axis and two long axes, and ellipsoid 3 (tri-axial; e3) has three axes of different radii. With volume normalization, the shapes (spheres: s1n, s2n, s3n; ellipsoids: e1n, e2n, e3n) are all standardized to a volume of 1 $cm^3$, with the same number of point coordinates representing the surface

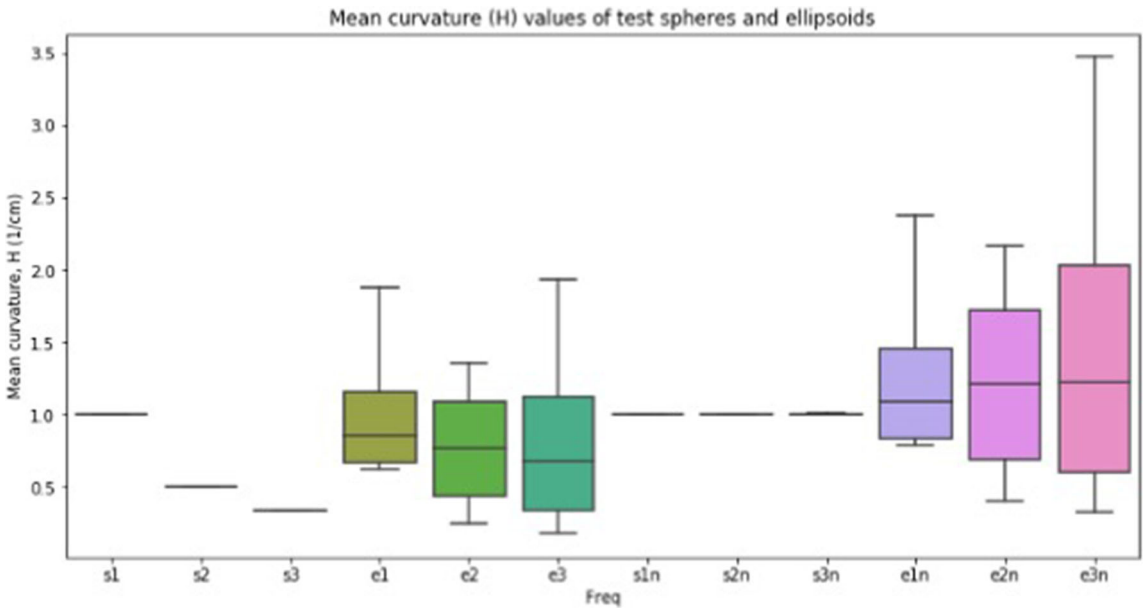


**Fig. 4** After scaling mean curvature values to a normalized volume (s1n to s3n, e1n to e3n), the pattern of distribution of mean curvature ($H$) remained unchanged, demonstrated by the constant shape of the corresponding box-plots. Naming conventions as in Fig. 1

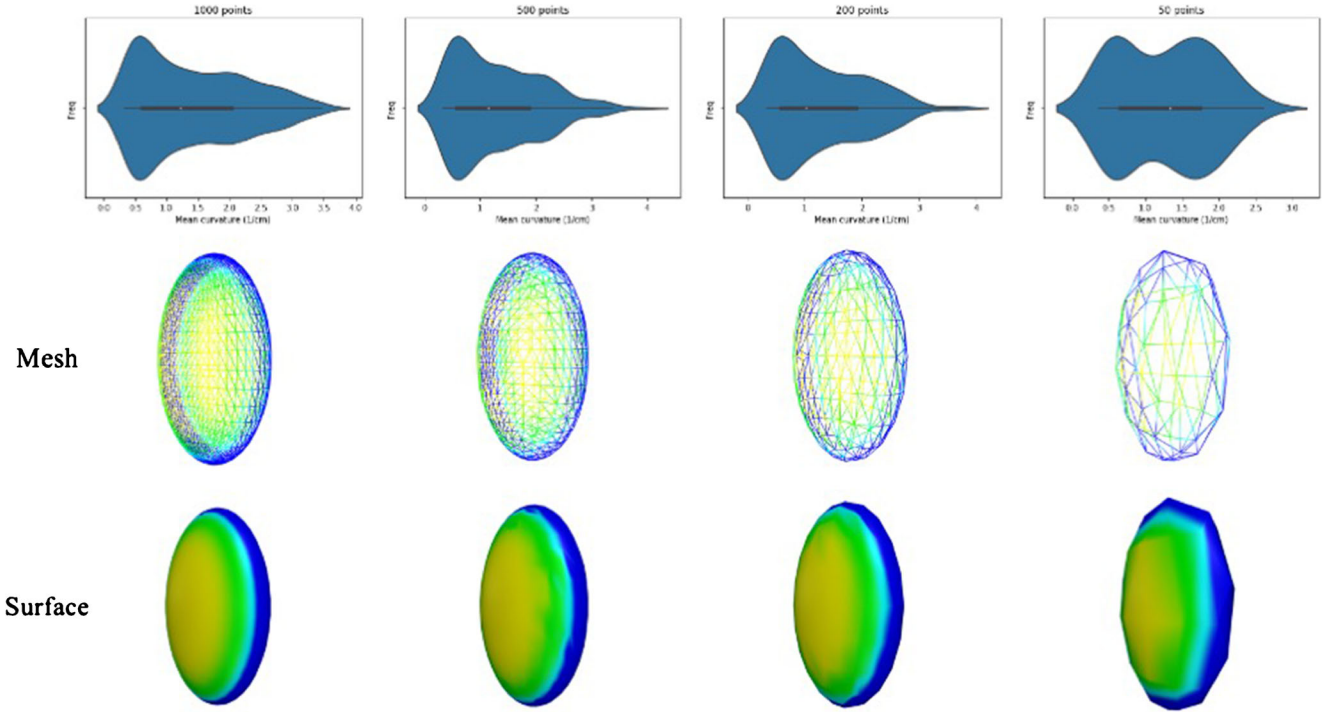


**Fig. 5** Effects of mesh density on frequency distribution of mean curvatures. The frequency distributions of mean curvatures remain generally preserved with reducing number of point samples, until there are too few points to accurately represent a shape, as in the case of 50 points

## Pilot tests

### Spheres and volume-normalized spheres

The mesh volumes of sphere and ellipsoids showed minor underestimation as compared to mathematically calculated volumes (Fig. 3). Before volume normalization, the mean curvatures for the 1-cm, 2-cm, and 3-cm-radius spheres were 1 $cm^{-1}$ (i.e., 1/1 cm), 0.5 $cm^{-1}$ (i.e., 1/2 cm), and 0.33 $cm^{-1}$ (i.e., 1/3 cm) respectively. Following volume normalization to that of a 1-cm-radius sphere, all spheres had mean curvature values of 1 $cm^{-1}$ (Fig. 4). For the ellipsoids, volume normalization did not alter the

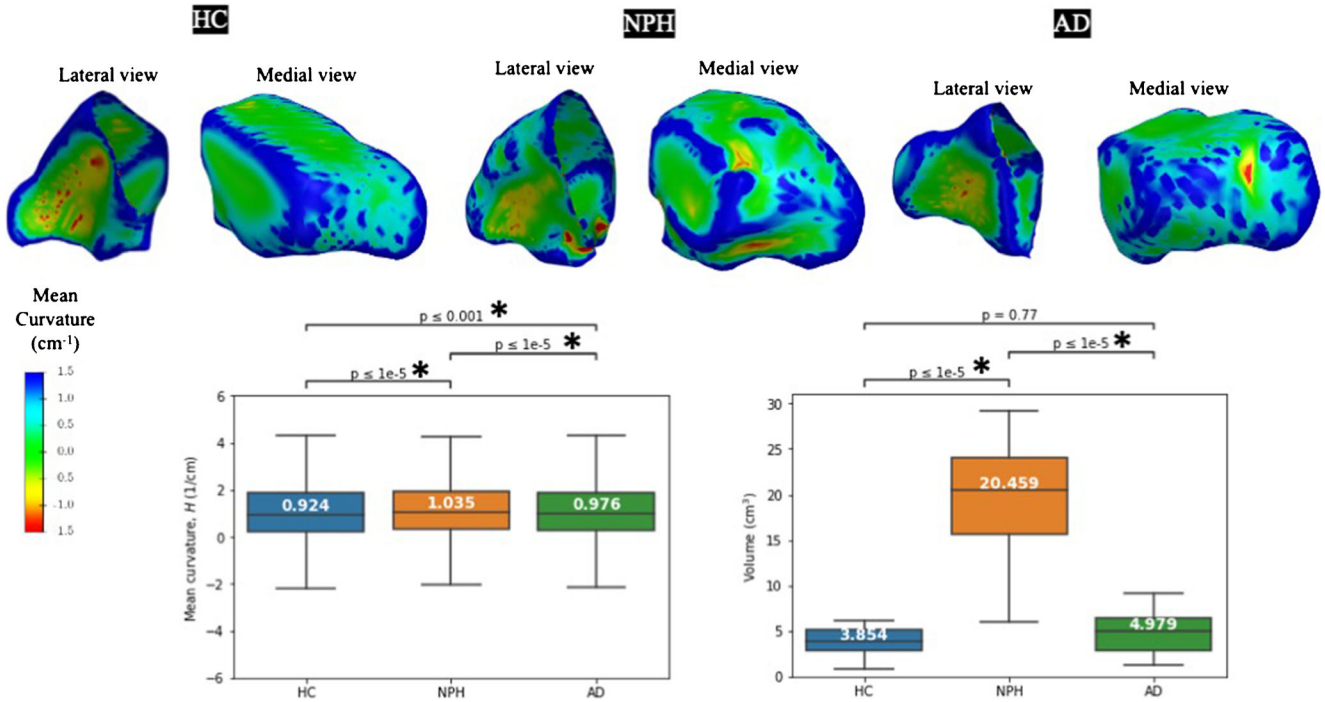


**Fig. 6** Mean curvature frequency distribution of left frontal horn of a healthy control (HC) subject and that of a normal pressure hydrocephalus (NPH) subject. All volumes had been normalized to the volume of the average left frontal horn derived from the HC group (3.9 $cm^3$)

distribution pattern of its surface curvature, evidenced by the preserved shapes of the box-and-whisker plots (Fig. 4).

### Effect of mesh density

Mesh density was determined by the number of point coordinates (vertices) representing a surface. Simulations with decreasing mesh density with an ellipsoid showed stability of the surface curvature distribution, although once the number of vertices became too small to accurately represent a shape, the surface curvature distribution became significantly altered (Fig. 5).

## Comparisons between HC, NPH, and AD

### Volumes

NPH subjects had a larger frontal horn (median: 20.5 $cm^3$) than HC subjects (3.9 $cm^3$; $p < 0.001$) and AD subjects (5.0 $cm^3$; $p < 0.001$) (Fig. 6). Volumetric analysis failed to differentiate AD from HC ($p = 0.77$).

### Mean surface curvature (*H*)

NPH subjects had an overall more rounded frontal horn than HC subjects (median $H$ 1.035 $cm^{-1}$ versus 0.924 $cm^{-1}$, respectively; $p < 0.001$) (Fig. 6). AD patients also had a more rounded frontal horn than HC subjects (median $H$ 0.976 $cm^{-1}$ versus 0.924 $cm^{-1}$, respectively; $p < 0.001$), although the difference was smaller in magnitude than that between HC and NPH.

Representing the respective distributions in the scatterplot with the volume as an additional dimension (Fig. 7), the NPH group was clearly identifiable as a distinct cluster, with higher median $H$ and volume (as per Fig. 6). The difference was more subtle between AD and HC cohorts: 13 of the 21 HC patients had a median $H$ below approximately 1 $cm^{-1}$ in the HC cohort, versus only 7 of the 21 patients in the AD group. Interestingly, for the AD and HC groups, as the ventricular volume increased, the median $H$ also increased (i.e., the ventricles became rounder). By contrast, this positive correlation was not observed for NPH ventricles.

### Regional curvature analysis

For the superolateral surface, both NPH and AD patients had rounder surfaces (median $H$ 1.034 $cm^{-1}$ and 0.856 $cm^{-1}$ respectively) than HC subjects (median $H$ 0.764 $cm^{-1}$; $p < 0.001$ and $p < 0.001$ respectively) (Fig. 8). NPH patients had a rounder superolateral surface than AD patients ($p < 0.001$).

For the superomedial surface, NPH patients exhibited a flattening of curvature in this region as compared to HC subjects ($H$ 0.686 $cm^{-1}$ versus 0.798 $cm^{-1}$, $p < 0.001$). There was no difference between AD and HC subjects ($H$ 0.783 $cm^{-1}$ versus 0.798 $cm^{-1}$, $p = 1.00$). NPH patients had a flatter superomedial surface than AD patients ($p < 0.01$).

For the inferolateral surface, both NPH and AD patients had rounder surfaces (median $H$ 1.102 $cm^{-1}$ and 0.914 $cm^{-1}$ respectively) than HC subjects (median $H$ 0.788 $cm^{-1}$; $p < 0.001$ and $p < 0.01$ respectively). NPH patients had a rounder inferolateral surface than AD patients ($p < 0.001$).

For the inferomedial surface, NPH patients had rounder surfaces (median $H$ 1.032 $cm^{-1}$) than HC subjects ($H$ 0.93

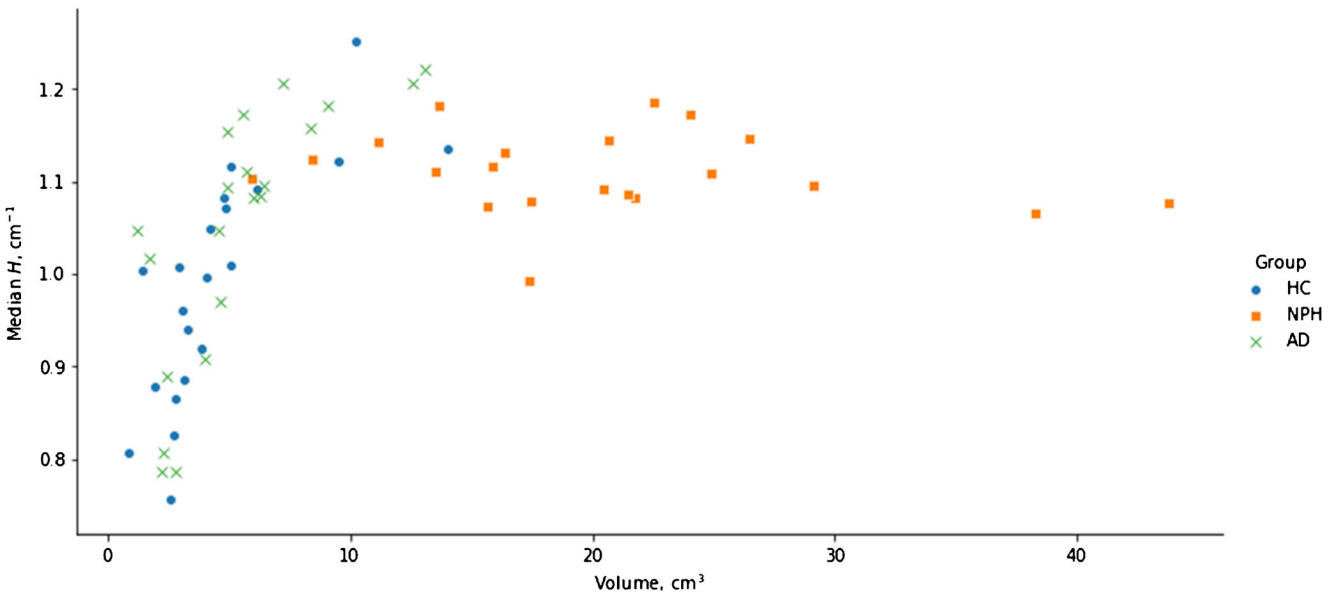


**Fig. 7** The distribution of mean curvature against volume. The normal pressure hydrocephalus (NPH), Alzheimer's disease (AD), and healthy control (HC) cohorts are identifiable as distinct clusters based on their curvature-volume characteristics

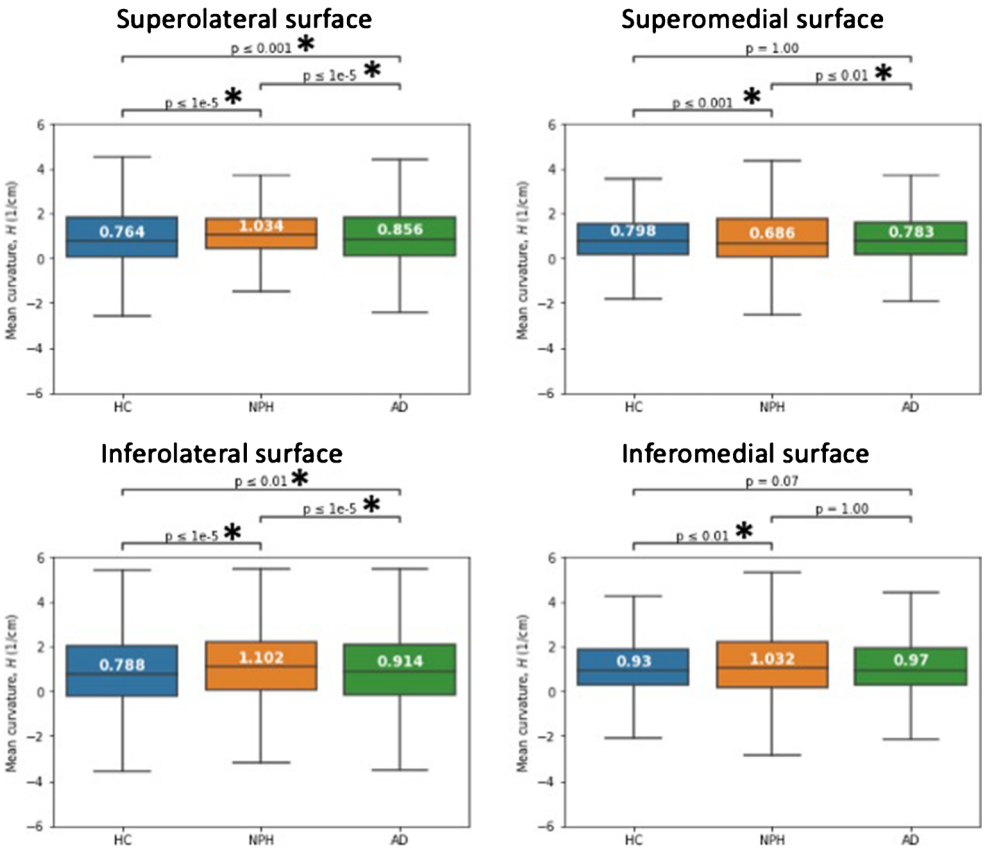


**Fig. 8** The mean curvature of the superolateral, superomedial, inferolateral, and inferomedial surfaces in healthy control (HC), normal pressure hydrocephalus (NPH), and Alzheimer's disease (AD)

$cm^{-1}$; $p < 0.01$). There was no difference between AD and HC subjects ($p = 0.07$) or between NPH and AD patients ($p = 1.00$).

### Curvature ratios (*R*)

Overall, the frontal horns in both NPH and AD were more rounded than HC subjects, by 12% ($R_{NPH}$ 1.12) and 6% ($R_{AD}$ 1.06) respectively (Table 1).

In NPH, the lateral surfaces (i.e., superolateral and inferolateral) increased in mean curvature by 35% and 40% ($R_{NPH}$ 1.35 and 1.40), respectively, as compared to those in HC subjects. The inferomedial surface increased in mean curvature by only 11% ($R_{NPH}$ 1.11). There was a flattening of the superomedial surface by 14% ($R_{NPH}$ 0.86) (Table 1).

In AD, the lateral surfaces also became more rounded as compared to HC subjects, although not to the same extent as NPH ($R_{NPH}$ 1.12 and 1.16). As mentioned above, there was no difference in the curvature of the medial surfaces between AD and HC.

## Discussion

In this pilot study, we profiled the surface mean curvature of the left anterior horn and compared the pattern of distortion in healthy controls, patients with normal pressure hydrocephalus, and those with Alzheimer's disease. The ventricle deforms unevenly, due to anatomical constraints from periventricular structures with differing compliance. Since CSF pressure within the ventricle equilibrates across the compartment, differences in curvature directly translate to differences in tissue distortion in the surrounding structures—a gentle curvature, in principle, distributes this distortion across a larger area, whereas a sharp curvature focuses the distortion over a small area. In our study, there was a rounding of the superolateral, inferolateral, and inferomedial surfaces, and a flattening of the superomedial surface, in those with ventriculomegaly, as compared to normal subjects. We found that significant differences in the mean curvature of lateral

**Table 1** Median mean curvature (*H*) values in HC, NPH, and AD groups. The curvature ratios (*R*) were defined as the ratio of median *H* in NPH ($R_{NPH}$) and AD ($R_{AD}$) compared to the median *H* in HC subjects; it is a measure of relative "roundedness" of the surface in diseased state as compared to a normal state

| | Median $H_{HC}$ | Median $H_{NPH}$ | Median $H_{AD}$ | $R_{NPH}$ | $R_{AD}$ |
|---|---|---|---|---|---|
| Overall | 0.924 | 1.035 | 0.976 | 1.12 | 1.06 |
| Superolateral | 0.764 | 1.034 | 0.856 | 1.35 | 1.12 |
| Superomedial | 0.798 | 0.686 | 0.783 | 0.86 | 0.98 |
| Inferolateral | 0.788 | 1.102 | 0.914 | 1.40 | 1.16 |
| Inferomedial | 0.930 | 1.032 | 0.970 | 1.11 | 1.04 |

surfaces (rounding of superolateral and inferolateral quadrants) were able to distinguish patterns of ventricular distortion between all three cohorts. Significant flattening of the superomedial surface was able to discriminate between cohorts of NPH compared to healthy controls and AD respectively. However, significant rounding of the inferomedial surface compared to controls was a distinguishing feature of NPH cohorts alone.

## Normal pressure hydrocephalus

In NPH, we found that the frontal horn predominantly dilated laterally. This manifested in the rounding of the lateral surfaces, by 35% (superolaterally) and 40% (inferolaterally) as quantified through our analysis. On the superomedial surface, there was a flattening of curvature, and here represent the topographical equivalent to tight high convexity and acute callosal angles, both well-described findings in NPH [2, 3, 25].

It remains to be evaluated whether the degree of rounding correlates with clinical outcomes and other parameters, and more studies are in progress. A positive correlation between the mean curvature (after volume normalization) and volume was seen for AD and HC frontal horns. For NPH, the mean surface curvature remained relatively constant even with increasing ventricular volume (Fig. 7). One explanation could be that as the ventricles progressively dilate in NPH, white matter tracts are first to be stretched as the ventricles distort and become rounder. However, after maximal rounding of the ependyma of the ventricles, further distortion becomes transmitted to deep grey matter, which would likely be less compliant than the white matter microstructure. This differential pattern of ventricular dilatation may partly explain the wide spectrum of clinical manifestations of NPH as well as the spectrum of reversibility of neural injuries. Further work is required to test this hypothesis.

## Alzheimer's disease

In AD, ventricular dilatation is a result of general cortical atrophy. We estimated that the frontal horns of AD were, on average, 6% more rounded than that of normal subjects. As compared to the normal subject, only the lateral surfaces were more rounded, while there was no difference in the medial surfaces. This was consistent with the mechanism of cortical atrophy driving ventriculomegaly, resulting in the expansion of ventricles lateralward, in the direction of the atrophied cortices.

## Curvature ratio (*R*)

The ventricle distends to a varying degree along different surfaces, owing to different compliance of the periventricular parenchyma. Using curvature analysis, the "roundedness" of a surface, relative to normal condition, could be quantified using an index like the proposed curvature ratio, *R*. *R* greater than 1 indicates relative rounding of the surface in a diseased state as compared to normal "healthy" individuals, whereas *R* lesser than 1 indicates relative flattening of the surface in a diseased state.

## Anatomical correlates

We conjecture that the described topographical differences could broadly represent two types of abnormalities in the periventricular parenchyma: neural stretching and structural compression.

Periventricular white matter abnormalities have been well-described in NPH [26]. Diffusion tensor imaging (DTI) and tractography could be correlated to topological changes to confirm the relationship between ventricular surface distortion and white matter tract deformation. With regards to structural compression, for example in NPH, reduction in the volume and perfusion of the caudate nucleus and thalamus had been reported [27, 28]; the integrity of surrounding structures may be determined by both the degree of volumetric change and the pattern of differential curvature distortion produced in the evolution of progressive ventriculomegaly. Ventricular distortion could conceivably precede caudate and thalamus atrophy, and abnormal patterns of progressive distension could have prognostic implications for the trajectory of the disease.

## Strengths and limitations

Our methodology utilized open-source software, based on 3D Slicer and Python-based modules. This enables reproducibility and transparency. All ventricles were volume-normalized, eliminating volume differences as a confounding factor. The description of surface topology may be superior to volumetric analysis as a tool to distinguish between cohorts of NPH versus normal aging and neurodegeneration. Further work has been planned, including the correlations with a more comprehensive examination of ventricular morphology, further segmentation of ventricular anatomical segments, and volumetric assessment of subcortical and cortical changes, to better examine the differential capacity for ventricular segments to deform in hydrocephalus.

Various potential sources of measurement error could have been introduced. Firstly, our method of ventricular segmentation was a semi-automated process; CSF-intensity voxels were first automatically identified, followed by manual exclusion of extraventricular CSF spaces that were falsely included during initial processing. The latter commonly included, for instance, the cisternal spaces in the regions of the sella turcica, pre-lamina terminalis cistern, quadrigeminal cistern, and cistern of the velum interpositum. However, these regions were not examined in this pilot study involving the frontal horn, a relatively consistent area to segment. Inter-operator variability in segmentation was possible but minimized by the use of a descriptive standard operating protocol of steps undertaken for

quality assurance, based on pilot testing. Additionally, surface modeling using approximate point coordinates and triangulated mesh, although a well-described technique that has been used in medical imaging processing in other fields [15, 16, 19], could result in subtle inaccuracies and underestimation of the volume, although based on pilot testing the discrepancies were insignificant. Other options to approximate curvature would include (1) local surface fitting techniques to reconstruct a surface, such as fitting a quadratic polynomial function to point coordinates [29, 30]; however, this would be computationally inefficient with minimal increase in accuracy, (2) tensor-based methods by calculating the average of curvature tensors over small areas [31, 32], although significant errors had been reported with this technique. To minimize the introduction of cumulative measurement errors, we restricted our analyses to the left frontal horn in this study. Further work is needed to extrapolate our findings to other topological segments of the ventricles.

### Future directions

Future studies should correlate these findings to clinical parameters and outcomes, as well as to radiological findings from other modalities of analysis. With regards to surgical shunting, topographical changes in ventricular curvature may offer a more sensitive measure than changes in CSF volume in predicting the response to shunting. Future studies should be conducted to evaluate the correlation between volumetric and linear measurements (such as Evan's index, bicaudal ratio, callosal angle) and topographical measurements. We believe the two methodologies to be complementary. Differential patterns of surface distortion, evaluated through standardized regional topographical analyses, may provide more granularity and supplement the traditional volumetric and linear indices in best describing ventricular morphology. Subtle morphological changes not otherwise detectable with linear indices and volumetric analysis could be a potential biomarker for correlation to neurological recovery, although it would still depend on other factors such as the structural integrity of deep nuclei and white matter tracts. Lastly, this technique could be considered a measure of hydrocephalic dilatation, which may or may not be specific to the condition of NPH. It may be possible to extend the technique to interrogate other conditions with a deformational difference in hydrocephalic patterns, such as differences in pediatric and adult post-hemorrhagic deformation and other forms of brain atrophy, to determine whether differences are due to hydrocephalus alone or specific to unique deformational changes with NPH.

## Conclusion

NPH ventricles deform non-uniformly, and the pattern of surface distortion may be used as an additional diagnostic tool to differentiate between these hydrocephalic conditions. The surface topology may have important clinical correlates and further study could be done to further characterize this.

**Supplementary Information** The online version contains supplementary material available at https://doi.org/10.1007/s00234-021-02698-8.

**Author Contributions** NCK and YTL conceptualized the experimental design and led revisions of the manuscript; YTL and LT analysed the data; YTL wrote the manuscript, and provided visualizations for the data. LT contributed to data acquisition and imaging processing. SK provided comments on the experimental design and revision of the manuscript. All authors reviewed the final manuscript.

**Funding** Nicole C Keong was supported by grants from the National Medical Research Council (NMRC/TA/0024/2013) and the National Neuroscience Institute Centre Grant (NCG CS03). Data collection and sharing for the ADNI project was funded by the Alzheimer's Disease Neuroimaging Initiative (ADNI) (National Institutes of Health Grant U01 AG024904) and DOD ADNI (Department of Defense award number W81XWH-12-2-0012). ADNI is funded by the National Institute on Aging, the National Institute of Biomedical Imaging and Bioengineering, and through generous contributions from the following: AbbVie, Alzheimer's Association; Alzheimer's Drug Discovery Foundation; Araclon Biotech; BioClinica, Inc.; Biogen; Bristol-Myers Squibb Company; CereSpir, Inc.; Cogstate; Eisai Inc.; Elan Pharmaceuticals, Inc.; Eli Lilly and Company; EuroImmun; F. Hoffmann-La Roche Ltd. and its affiliated company Genentech, Inc.; Fujirebio; GE Healthcare; IXICO Ltd.; Janssen Alzheimer Immunotherapy Research & Development, LLC.; Johnson & Johnson Pharmaceutical Research & Development LLC.; Lumosity; Lundbeck; Merck & Co., Inc.; Meso Scale Diagnostics, LLC.; NeuroRx Research; Neurotrack Technologies; Novartis Pharmaceuticals Corporation; Pfizer Inc.; Piramal Imaging; Servier; Takeda Pharmaceutical Company; and Transition Therapeutics. The Canadian Institutes of Health Research is providing funds to support ADNI clinical sites in Canada. Private sector contributions are facilitated by the Foundation for the National Institutes of Health (www.fnih.org). The grantee organization is the Northern California Institute for Research and Education, and the study is coordinated by the Alzheimer's Therapeutic Research Institute at the University of Southern California. ADNI data are disseminated by the Laboratory for Neuro Imaging at the University of Southern California.

## Declarations

**Conflict of interest** The authors declare that they have no additional conflict of interest.

**Ethical approval** The study was approved by the National Healthcare Group Domain Specific Review Board (Ref 2014/00838) and the SingHealth Centralised Institutional Review Board (Ref 2016/2627).

**Informed consent** Informed consent was obtained from all individual participants included in the study.

## References

1. Evans WA (1942) An encephalographic ratio for estimating ventricular enlargement and cerebral atrophy. Arch Neurol Psychiatr 47:931–937. https://doi.org/10.1001/archneurpsyc.1942.02290060069004

2. Virhammar J, Laurell K, Cesarini KG, Larsson EM (2014) The callosal angle measured on MRI as a predictor of outcome in idiopathic normal-pressure hydrocephalus. J Neurosurg 120:178–184. https://doi.org/10.3171/2013.8.JNS13575
3. Sjaastad O, Nordvik A (1973) The corpus callosal angle in the diagnosis of cerebral ventricular enlargement. Acta Neurol Scand 49:396–406. https://doi.org/10.1111/j.1600-0404.1973.tb01312.x
4. Yamada S, Ishikawa M, Yamamot K (2015) Optimal diagnostic indices for idiopathic normal pressure hydrocephalus based on the 3D quantitative volumetric analysis for the cerebral ventricle and subarachnoid space. Am J Neuroradiol 36:2262–2269. https://doi.org/10.3174/ajnr.A4440
5. Kitagaki H, Mori E, Ishii K et al (1998) CSF spaces in idiopathic normal pressure hydrocephalus: Morphology and volumetry. AJNR Am J Neuroradiol 19(7):1277–1284
6. Keong NCH, Pena A, Price SJ et al (2016) Imaging normal pressure hydrocephalus: theories, techniques, and challenges. Neurosurg Focus 41:E11. https://doi.org/10.3171/2016.7.FOCUS16194
7. Palm WM, Walchenbach R, Bruinsma B, Admiraal-Behloul F, Middelkoop HA, Launer LJ, van der Grond J, van Buchem M (2006) Intracranial compartment volumes in normal pressure hydrocephalus: volumetric assessment versus outcome. Am J Neuroradiol 27:76–79
8. Keong NC, Pena A, Price SJ, Czosnyka M, Czosnyka Z, DeVito EE, Housden CR, Sahakian BJ, Pickard JD (2017) Diffusion tensor imaging profiles reveal specific neural tract distortion in normal pressure hydrocephalus. PLoS One 12:e0181624. https://doi.org/10.1371/journal.pone.0181624
9. Peña A, Owler BK, Fryer TD, Minhas P, Czosnyka M, Crawford PJ, Pickard JD (2002) A case study of hemispatial neglect using finite element analysis and positron emission tomography. J Neuroimaging 12:360–367. https://doi.org/10.1111/j.1552-6569.2002.tb00145.x
10. Relkin N, Marmarou A, Klinge P et al (2005) INPH guidelines, part II: diagnosing idio-pathic normal-pressure hydrocephalus. Neurosurgery 57:S2-4–S2-16. https://doi.org/10.1227/01.NEU.0000168185.29659.C5LK
11. Morris JC (1997) Clinical dementia rating: a reliable and valid diagnostic and staging measure for dementia of the Alzheimer type. In: International Psychogeriatrics. Int Psychogeriatr 9(Suppl 1):173–176; discussion 177–8. https://doi.org/10.1017/s1041610297004870
12. McKhann GM, Knopman DS, Chertkow H et al (2011) The diagnosis of dementia due to Alzheimer's disease: recommendations from the National Institute on Aging-Alzheimer's Association workgroups on diagnostic guidelines for Alzheimer's disease. Alzheimers Dement 7:263–269. https://doi.org/10.1016/j.jalz.2011.03.005
13. Petersen RC, Aisen PC, Beckett LA, Donohue MC, Gamst AC, Harvey DJ, Jack CR, Jagust WJ, Shaw LM, Toga AW, Trojanowski JQ, Weiner MW (2010) Alzheimer's disease neuroimaging initiative (ADNI): Clinical characterization. Neurology 74 (3):201–209
14. Kikinis R, Pieper SD, Vosburgh KG (2014) 3D Slicer: A platform for subject-specific image analysis, visualization, and clinical support. In: Jolesz F. (eds) Intraoperative imaging and image-guided therapy. Springer, New York, NY. https://doi.org/10.1007/978-1-4614-7657-3_19
15. Addetia K, Maffessanti F, Yamat M, Weinert L, Narang A, Freed BH, Mor-Avi V, Lang RM (2016) Three-dimensional echocardiography-based analysis of right ventricular shape in pulmonary arterial hypertension. Eur Heart J Cardiovasc Imaging 17:564–575. https://doi.org/10.1093/ehjci/jev171
16. Addetia K, Maffessanti F, Muraru D, Singh A, Surkova E, Mor-Avi V, Badano LP, Lang RM (2018) Morphologic analysis of the normal right ventricle using three-dimensional echocardiography–derived curvature indices. J Am Soc Echocardiogr 31:614–623. https://doi.org/10.1016/j.echo.2017.12.009
17. Musy M, Dalmasso G, Bane S (2019) vtkplotter, a python module for scientific visualization and analysis of 3D objects and point clouds based on VTK (Visualization Toolkit), Zenodo. https://doi.org/10.5281/zenodo.2561402
18. Garland M, Heckbert PS (1997) Surface simplification using quadric error metrics. Proc 24th Annu Conf Comput Graph Interact Tech SIGGRAPH 1997 209–216. https://doi.org/10.1145/258734.258849
19. Sciancalepore MA, Maffessanti F, Patel AR, Gomberg-Maitland M, Chandra S, Freed BH, Caiani EG, Lang RM, Mor-Avi V (2012) Three-dimensional analysis of interventricular septal curvature from cardiac magnetic resonance images for the evaluation of patients with pulmonary hypertension. Int J Card Imaging 28:1073–1085. https://doi.org/10.1007/s10554-011-9913-3
20. Batchelor P, Maclean A, Batchelor P, Maclean A (2020) vtkCurvatures class reference
21. Mesmoudi MM, De Floriani L, Magillo P (2012) Concentrated curvature for mean curvature estimation in triangulated surfaces. Lect Notes Comput Sci (including Subser Lect Notes Artif Intell Lect Notes Bioinformatics) 7309 LNCS:79–87. https://doi.org/10.1007/978-3-642-30238-1_9
22. Gray A, Abbena E, Salamon S (2017) Modern differential geometry of curves and surfaces with Mathematica, 3rd Edition
23. Rypl D, Bittnar Z (2006) Generation of computational surface meshes of STL models. J Comput Appl Math 192:148–151. https://doi.org/10.1016/j.cam.2005.04.054
24. Dyn N, Hormann K, Kim S, Levin D (2001) Optimizing 3D triangulations using discrete curvature analysis. Mathematical Methods for Curves and Surfaces: Oslo 2000 135. Tom Lyche and Larry L. Schumaker (eds.), pp. 135–146
25. Ishii K, Kanda T, Harada A, Miyamoto N, Kawaguchi T, Shimada K, Ohkawa S, Uemura T, Yoshikawa T, Mori E (2008) Clinical impact of the callosal angle in the diagnosis of idiopathic normal pressure hydrocephalus. Eur Radiol 18:2678–2683. https://doi.org/10.1007/s00330-008-1044-4
26. Mataró M, Matarín M, Poca MA et al (2007) Functional and magnetic resonance imaging correlates of corpus callosum in normal pressure hydrocephalus before and after shunting. J Neurol Neurosurg Psychiatry 78:395–398. https://doi.org/10.1136/jnnp.2006.096164
27. DeVito EE, Salmond CH, Owler BK et al (2007) Caudate structural abnormalities in idiopathic normal pressure hydrocephalus. Acta Neurol Scand 116:328–332. https://doi.org/10.1111/j.1600-0404.2007.00906.x
28. Bateman GA (2008) The pathophysiology of idiopathic normal pressure hydrocephalus: cerebral ischemia or altered venous hemodynamics? Am J Neuroradiol 29:198–203. https://doi.org/10.3174/ajnr.A0739
29. Zhong L, Yeo SY, Su Y, et al (2007) Regional assessment of left ventricular surface shape from magnetic resonance imaging. In: Annual International Conference of the IEEE Engineering in Medicine and Biology – Proceedings, pp 884–887
30. Garimella R, Swartz B (2003) Curvature estimation for unstructured triangulations of surfaces. Los Alamos Natl Lab 836:0–10
31. Batagelo HC, Wu ST (2007) Estimating curvatures and their derivatives on meshes of arbitrary topology from sampling directions. Visual Comput 23:803–812. https://doi.org/10.1007/s00371-007-0133-8
32. Alliez P, Cohen-Steiner D, Devillers O, et al (2003) Anisotropic polygonal remeshing. ACM Transactions on Graphics, Association for Computing Machinery 22(3):485–493